Generic guiding principle for the prediction of metal-induced reconstructions of compound semiconductor surfaces

Shenyuan Yang,[1,2] Lixin Zhang,[1] Hua Chen,[2] Enge Wang,[1] and Zhenyu Zhang[3,2]

[1]*International Center for Quantum Structures and Institute of Physics, Chinese Academy of Sciences, Beijing 100190, People's Republic of China*
[2]*Department of Physics and Astronomy, The University of Tennessee, Knoxville, Tennessee 37996, USA*
[3]*Materials Science and Technology Division, Oak Ridge National Laboratory, Oak Ridge, Tennessee 37831, USA*

We have performed extensive and systematic *ab initio* calculations to substantiate a recently proposed generalized electron counting (GEC) rule that governs the rich patterns of compound semiconductor reconstruction induced by metal adsorption. In this rule, the metal adsorbates serve as an electron bath, either donating or accepting the right number of electrons, with which the binary host system chooses a specific reconstruction under the classic electron counting rule and, meanwhile, the adsorbates stay in their optimal valency. The GEC rule is applied to different GaAs surfaces deposited by various classes of metal adsorbates, leading to a number of possible reconstructions, which can be further confirmed by first-principles calculations and/or experiments. The alkali-metal adsorption on the GaAs(110) surface up to the saturate coverage is a perfect example of the GEC rule. The application of the GEC rule to the prototype system of Mn/GaAs(001) not only predicts possible reconstruction patterns over a wide range of coverage but also provides an underlying link between the reconstruction structures and the local magnetic moments of the metal adsorbates. For Au/GaAs(100), we demonstrate the application of the GEC rule to those systems where metal adsorbates form covalent bonds with the substrate. The GEC rule, as a generic principle, is expected to be applicable to more metal-adsorbed compound semiconductor surfaces.

PACS number(s): 68.35.−p, 68.43.Bc, 75.70.−i

I. INTRODUCTION

Surface reconstruction and the special case of surface relaxation are fundamental issues in surface physics. An ideal semiconductor surface is unstable due to the broken bonds that contain unpaired electrons. In order to lower the surface free energy, the atoms in the top layers relax from their truncated positions and sometimes form new bonds, leading to a reconstructed surface. In addition, the reconstructed surface may have a different stoichiometry from the bulk to satisfy the requirement that the surface region be charge neutral. For compound semiconductors such as GaAs, a simple electron counting (EC) model[1] has been developed and proven to be extraordinarily instrumental in recognizing a wide variety of surface reconstructions. According to the EC model, the bonding and nonbonding surface states below the Fermi energy must be filled while the nonbonding and antibonding states above the Fermi energy must be empty, minimizing the free energy of the surface. Given the number of available electrons, a surface structure obeying the EC rule will have all the dangling bonds on the electronegative element full and all those on the electropositive element empty, leaving no net surface charge. For a specific surface, this rule selects a set of energetically favored structures from which the actual one can be further determined by experiments and theoretical calculations. Since its proposal, the EC model has been successfully applied to various homogeneous semiconductor systems and determined a large number of surface reconstructions.[2,3] It has also been proven to be instrumental in the identification of the structures of the surface defects such as vacancies, steps and islands,[4] and even in the description of the homoepitaxial growth mode.[5]

Metal/semiconductor heterogeneous interfaces are indispensable to technological applications in microelectronics and optoelectronics, such as transistors and interconnects. Recently, ferromagnetism/semiconductor heterostructures and diluted magnetic semiconductors (DMS) (Ref. 6) became a topic of interest since it is anticipated that such structures can lead to the integration of magnetism and semiconductor electronics. These materials are often obtained by epitaxial growth. At the initial stages of growth, the semiconductor substrate deposited with a submonolayer of metal often exhibits much richer and more complex reconstruction patterns than the corresponding homogeneous surface. For instance, at low coverage, alkali metals (AMs) form one-dimensional (1D) long chains on III–V(110) surfaces in the $[1-1\ 0]$ direction.[7–10] Deposition of Sb_4 on GaAs(110)-$\beta 2(2 \times 4)$ surface produces a (2×8) reconstruction that turns to a (2×4) surface upon annealing[11] whereas adsorption of Mn on the same substrate leads to a smaller (2×2) reconstruction.[12] Not only are the atomic structures of these reconstructions interesting in themselves but also they influence the metal/semiconductor contacts such as the smoothness of the interface, the optimization of the growth of the epitaxial films, the Fermi energy pinning, and the Schottky barrier heights.[13] However, further understanding of the reconstruction patterns is hindered by the complexity of the interactions at the interface induced by the metal adsorbates. Despite the persistent efforts to gain complete understanding of these heterogeneous systems,[14] there is still a lack of a generic guiding principle in interpreting or predicting the diverse patterns of metal-induced reconstructions.

In a recent paper,[15] we proposed a generalized electron counting (GEC) rule to explain a wide range of metal-

induced compound semiconductor reconstructions. Briefly, in the GEC rule, the metal adsorbates serve primarily as an electron bath by donating or accepting the right number of electrons, as the host surface chooses a specific reconstruction that obeys the classic EC model. This generalization is rooted in the realization that metal atoms are generally far less demanding in forming directional chemical bonds and are more susceptible to charge transfer. Accordingly the metal adsorbates will play a flexible role in selecting a particular reconstruction. As its classic counterpart, the GEC rule can dramatically simplify the task of determining the reconstructions for a specific metal/semiconductor adsorption system by greatly narrowing down the number of possible structures out of many candidate patterns in configuration space. This has been a tough task so far, which refers to the comparison of massive trial-and-error theoretical calculations to experimental results.

One well-known and extensively used semiconductor, i.e., GaAs, is studied as the binary host system to demonstrate the power of the GEC rule in the interpretation and prediction of the metal-induced reconstructions. A number of reconstruction patterns of the GaAs surfaces with a broad range of metal adsorbates, including the most electropositive AMs, magnetic element Mn, and the noble metal Au, are systematically studied over a wide range of coverage. The GEC predictions are further confirmed by first-principles calculations and comparisons with available experiments. Under the guidance of the GEC rule, the adsorption behaviors of the AMs on GaAs(110) surface are well explained. Group-III and group-V metals behave just as Ga and As, respectively, leading to an extension of the classic EC model. For magnetic adsorbates Mn, the GEC rule can predict possible low-energy reconstructions over a wide range of coverage. Moreover, an intrinsic link between the specific surface reconstructions and the local magnetic moment of the adsorbates can be established based on the GEC rule. Since the total magnetic moment and the collective magnetic properties of the interface are intimately tied to the local magnetic moment of individual magnetic adsorbate, the GEC rule in principle provides a conceptual way to control the surface magnetism in Mn/GaAs(001) and other related systems[6] by manipulation of the reconstruction patterns. The electron counting technique can also be applied to other metal adsorbates such as Au that forms strong covalent bonds with the substrate.

The rest of this paper is organized as follows. After an introduction in Sec. I, the computational methods are given in Sec. II. In Sec. III we discuss the concept of the GEC rule and introduce a simple counting formula. From Secs. IV–VII the GEC rule is applied to different reconstructions of GaAs surfaces with various types of metal adsorbates: the AMs that are much less electronegative than Ga (Sec. IV), the trivalent *sp* metals whose electronegativities are close to Ga and the group-V metals whose electronegativities are close to As (Sec. V), the magnetic metal Mn (Sec. VI), and the noble metal Au (Sec. VII). Finally the conclusion is given in Sec. VIII.

II. COMPUTATIONAL METHODS

Our first-principles calculations are carried out using the Vienna *ab initio* simulation package (VASP) (Ref. 16) with the generalized gradient approximation (GGA) (Ref. 17) and a plane-wave basis set. Detailed computational settings depend on the specific metal/semiconductor systems. For AM/GaAs(110), we employ the all-electron-like projector-augmented wave (PAW) potentials[18] for their reliable description of the AMs. The cut-off energy in the plane-wave expansion is set to 200 and 300 eV for Cs and Na, respectively. We use a slab of ten-layer thickness with five layers of GaAs to model the GaAs(110) surface. The bottom side of the slab is passivated by pseudohydrogens with 5/4 or 3/4 electrons. The positions of the pseudohydrogens and the bottom-layer GaAs are kept fixed during the structure relaxation. Two kinds of supercell of 2×2 and 4×4 are used in the calculations, and the corresponding Monkhorst-Pack k-points[19] mesh for the Brillouin-zone summation is set as $4 \times 4 \times 1$ and $2 \times 2 \times 1$, respectively.

The spin-polarized calculations for Mn/GaAs(001) are performed with the Vanderbilt ultrasoft pseudopotentials.[20] The Mn $3d$ states are treated as the valence and the cut-off energy for the plane-wave basis is set to 200 eV. The Ga-terminated GaAs(001) 2×2 surface is modeled by an eight-bilayer slab with at least four GaAs bilayers, the bottom of which is passivated by pseudohydrogen atoms. The bottom-layer Ga and H are fixed during structure optimizations while all the other layers are fully relaxed. A $2 \times 2 \times 1$ k-points mesh is used for structure optimization and a more dense $8 \times 8 \times 1$ mesh for the density-of-states calculations.

For Au/GaAs(001) system, we use the ultrasoft pseudopotentials and treat Au $5d$ as valence states. The plane-wave cutoff is 200 eV. The computational parameters for Au on Ga-terminated 2×2 surface are similar to those used for Mn/GaAs(001) system. To model the As-terminated GaAs(001)-$\beta 2(2 \times 4)$ surface, we use a ten-bilayer thick supercell containing five bilayers of GaAs. A $4 \times 2 \times 1$ k-points mesh is used for relaxation and an $8 \times 4 \times 1$ mesh for density-of-states calculations. In addition, Au adsorption on a larger 4×4 supercell has also been calculated for comparison. We also test selective structures with PAW pseudopotentials and obtain the qualitatively same results.

III. GENERALIZED ELECTRON COUNTING RULE FOR GaAs

Let us start with a brief review of the classic EC model for clean GaAs surfaces. According to the EC model, each atom contributes a nominal fractional charge [=(number of valence electrons)/(number of bonds)] to each of the shared and dangling bonds. For zinc blende semiconductors such as GaAs, each atom forms four bonds with its neighbor atoms and thus a Ga atom contributes 3/4 of an electron while an As atom contributes 5/4 of an electron to each bond, leading to a total of $3/4 + 4/5 = 2$ electrons in each bond, as it should be. At an ideal surface, there are always partially occupied dangling bonds that serve as a driving force of the surface reconstruction such that all the dangling bonds on As atoms are filled and those on Ga atoms empty. On a clean GaAs(110) surface, charge transfer from the surface Ga dangling bond (3/4 occupied) to the As dangling bond (5/4 occupied) can nicely fulfill the EC require-
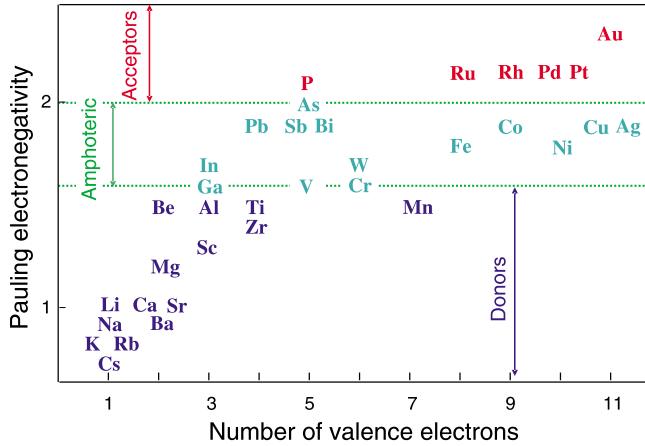
FIG. 1. (Color online) Pauling electronegativities of various metals with respect to that of Ga and As (Ref. 23).

ments. Consequently, the surface As and Ga atoms involve in s^2p^3- and sp^2-like configurations, respectively, leading to a surface relaxation with As upward and Ga inward.[2] The GaAs(001) surface, on the other hand, forms various reconstructions depending on the preparation conditions and the surface stoichiometry. In general, these reconstructions include: (1) formation of surface dimers, which are the primary structural motif at this surface, (2) arrangement of the dimers, and (3) charge transfer.[2,3] The As-terminated $\beta2(2 \times 4)$ structure was thought to be the most stable reconstruction under a wide range of growth conditions.

The first issue that concerns metal deposition on a compound semiconductor surface is the adsorption sites. From extensive literatures, we deduce a general trend of metal adsorption sites on semiconductor surfaces. The s and sp metals such as Cs and Au prefer the substitutional sites (including would-be-substitutional sites above the surface),[7,21] whereas the d-active metals such as Mn prefer the interstitial sites near the surface.[6,22] The site preference is rooted in the fact that the sp-metal atoms are likely to be involved in a sp^2 or sp^3 rehybridization and then bond with the surface atoms, which can be easily satisfied at substitutional sites. On the other hand, transition-metal atoms with d electrons prefer a complex multicoordination with other atoms, which is more easily fulfilled when they occupy the interstitial sites. The same trend holds for the GaAs substrate in our first-principles calculations.

Another important issue involves whether a metal adsorbate serves as a donor or acceptor within the ternary system according to its relative capability of attracting electrons, which can be quantitatively described by the electronegativity. Figure 1 shows the Pauling electronegativities of various metals compared to those of Ga and As.[23] Taking the electronegativity values of Ga and As as boundaries, the metals can be divided into three types. The alkali and alkaline metals marked in blue in Fig. 1 are more electropositive than both Ga and As, and are expected to behave as donors on GaAs surfaces. Thus even the dangling bonds on surface Ga may be filled with the help of these donor metals. In contrast, the metals marked in red are more electronegative than both Ga and As, and are thereby expected to behave as acceptors.

In the middle region, the metals, most of which are transition metals, have their electronegative values lying between those of Ga and As. Whether they serve as a donor or acceptor should be analyzed on a case-by-case basis. However, the transition metal Mn is a bit more electropositive than Ga and therefore is expected to act as a donor. Clearly different compound semiconductors have different electronegativity bounds and thus different classifications of potential donors and acceptors.

According to the GEC rule, for an arbitrary GaAs slab with metal adsorbates, we have

$$n_R = \nu_M n_M + 3n_{Ga} + 5n_{As} - 2n_{bonds}, \tag{1}$$

where n_M, n_{Ga}, and n_{As} are the number of metal, Ga, and As atoms in the slab, respectively; n_M as the number of valence electrons on an isolated metal atom, n_R the number of valence electrons remaining on the metal atoms for a specific reconstruction, and n_{bonds} the total number of chemical bonds in the slab, including the σ bonds and the occupied dangling bonds at the surface, i.e., $n_{bonds} = n_{\sigma\text{-bonds}} + n_{ODBs}$. The first three terms at the right of the equation are just the total number of valence electrons contained in the slab. Within the GEC picture, a candidate low-energy surface reconstruction must have the optimal values of n_R, which means the sp-metal atoms should have a filled electronic shell or subshell. More complexity arises for transition metals due to their diffusive d electrons where the optimal n_R may be system dependent. In the case of Mn/GaAs(001), our calculations show that each Mn atom is apt to donate its two s electrons to the substrate, leaving its half-filled d-shell intact, i.e., the optimal $n_R = 5$. This can be understood by the fact that a state with a larger spin will be energetically more favorable (Hund's rule). The value $(n_R - n_M n_M)$ measures the net charge transfer from the metal adsorbates to the substrate (if there are no covalent bonds between them): negative for donors and positive for acceptors. For a clean surface without metal adsorption, we have $n_M = 0$ and $n_R = 0$, and the GEC rule automatically reduces to the classic EC rule.

IV. ALKALI-METAL ADSORPTION ON GaAs(110)

Due to the simplicity of its electronic structures, alkali-metal adsorption on the III–V (110) surfaces has been widely investigated as a prototype of the metal-semiconductor interfaces.[13] AM/III–V (110) also provides a playground for probing the low dimensional systems and self-assembly.[10,24] Scanning tunneling microscopy (STM) studies have shown that on different III–V (110) surfaces Cs and K atoms form long 1D zigzag chains along $[1-1\ 0]$ direction at low coverage[7–10] while smaller Na atoms form much sparser linear chains.[25] Statistical distribution of the interchain distance as a function of coverage indicates the presence of a repulsive interaction among the chains in the [001] direction.[9,10] With the increase in the coverage, the adlayer develops to two-dimensional (2D) clusters and then to three-dimensional (3D) phase.[26] Scanning tunneling spectroscopy (STS) and electron energy loss spectroscopy (EELS) measurements suggested that the 1D chains and 2D adlayer are insulating, which can be interpreted by surface bipolaron or Hubbard
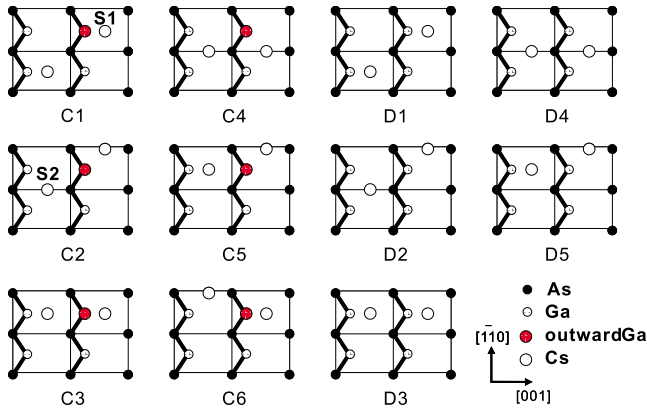
FIG. 2. (Color online) Configurations for the eleven dimer complexes with two Cs adsorbates on a GaAs(110) 2×2 surface cell, all of which are different combinations of S1 and S2 adsorption sites. The small black and small shaded balls are As and Ga atoms, respectively, large red shaded balls are the outward Ga atoms, and large balls are the Cs adsorbates.

FIG. 3. (Color online) The geometry and difference electron density $\Delta\rho$ for the building block of Cs chains on GaAs(110). The As, Ga, and Cs atoms are represented by yellow, gray, and green balls, respectively, and the outward *b*-Ga is highlighted with an arrow. The isosurfaces of $\Delta\rho$ is chosen to be ± 0.01 e/Å^3. Red and blue colors denote electron accumulation and depletion, respectively.

correlation,[8,27,28] whereas the 3D structure is metallic.[29] Ultraviolet photoelectron spectroscopies (UPS) showed two components in the Cs shifted core levels, and extra components in the anion and cation core levels, corresponding to two inequivalent adsorption sites for AM adatoms, and charge transfer between AM adatoms and substrate.[9,30,31] A number of theoretical calculations have investigated the atomic and electronic structures of these interfaces.[28,32,33] However, a unified picture to understand the experiments is still lacking. Here under the guidance of the GEC rule, we propose a building block for the AM chains based on which a unified explanation for many experimental results is obtained.

A. Building block of alkali-metal chains on GaAs(110)

Previous theoretical calculations[28] have confirmed that the AM adatom has a stable adsorption site S1 and a metastable site S2 on the III–V (110) surface, as shown in Fig. 2 C1 and C2, respectively. The S1 site is close to the epitaxial anion position while the S2 site is close to the epitaxial cation position. Since AM atoms do not intermix with the substrate, we adopt the above adsorption geometry in this paper. According to the classic EC rule, on a clean GaAs(110) surface all the dangling bonds on As are filled while those on Ga are empty. Thus the most electropositive AM adsorbates may donate their outer *s* electrons to the dangling bonds on Ga, as expected by the GEC rule. Since each AM atom has only one

valence electron, a stable motif of the AM-induced reconstruction should contain pairs of AM atoms.

First, we study the adsorption structures with two Cs atoms on a 2×2 GaAs(110) surface cell, corresponding to the coverage $\theta_{Cs} = 1/4$ monolayer (ML). We chose eleven configurations shown in Fig. 2 as the initial geometries, all of which are different possible combinations of S1 and S2 sites. The red larger circles in configurations C1–C6 represent the Ga atoms shifted higher than the surface As. D1–D5 are the corresponding configurations without Ga moving outward. In the following we refer these structures with two AM atoms as dimer complexes and denote them by DC_C1 to DC_D5. The total energies of these dimer complexes after full relaxation are listed in Table I. The following conclusions can be obtained from the calculations: (1) the configurations with one Ga moving outward are energetically more favorable than the ones without; (2) configuration C1, in which the two Cs atoms both occupy S1 sites and the Ga atom nearest to them [denoted by *b*-Ga in Fig. 3(a)] moves outward, is the most stable structure among all the configurations studied; and (3) most of the other configurations do not have very high energies, especially for those with one Ga moving outward with the maximum deviation only being 0.3 eV. We then extend our calculation to other systems, i.e., Na/GaAs(110) and Cs/InAs(110). Although the stability sequence of different dimer complexes is not the same for these systems, the above conclusions are qualitatively similar, i.e., DC_C1 is more favorable than all the other dimer complexes and can be assigned as the building block of AM chains.

TABLE I. Total energies of the eleven dimer complexes in unit of eV for Cs/GaAs(110), Na/GaAs(110), and Cs/InAs(110) systems. DC_C1 has the lowest energy among all these dimer complexes and its energy is assumed to be zero in each system. For Na/GaAs(110) and Cs/InAs(110), no stable geometries of DC_C6 or DC_C5 can be obtained and thus the corresponding values are not given.

	DC_C1	DC_C2	DC_C3	DC_C4	DC_C5	DC_C6	DC_D1	DC_D2	DC_D3	DC_D4	DC_D5
Cs/GaAs	0.0	0.23	0.15	0.22	0.09	0.30	0.10	0.67	0.15	0.71	0.29
Na/GaAs	0.0	0.43	0.24	0.35	0.24	0.39	0.38	0.69	0.51	0.67	
Cs/InAs	0.0	0.28	0.15	0.02	0.12		0.10	0.57	0.20	0.56	0.34

The difference between the configurations with one Ga outward and those without can be understood with the GEC rule. Take DC_C1 and DC_D1 as an example. As discussed above, a Cs adsorbate will donate its single s electron to the dangling bonds on Ga atoms since all the dangling bonds on As are full. In DC_D1, which is without Ga outward, the two Ga atoms next to Cs are equivalent. The two electrons donated by the two Cs adsorbates are thus supposed to be evenly distributed to the two Ga atoms; hence neither of the dangling bonds on Ga is saturated. However for DC_C1, the two Ga atoms next to Cs are inequivalent. And the two electrons donated by Cs can fully fill the dangling bond on b-Ga, leaving the other three empty, which is referred as the negative-U behavior of b-Ga.[28] Accordingly, the orbitals of b-Ga have to be rehybridized (from sp^2- to sp^3-like) such that the dangling-bond state shifts below the Fermi level, resulting in a local structure modification or derelaxation[32] around the b-Ga site (see Fig. 3). In other words, DC_C1 satisfies the GEC rule while DC_D1 doesn't and therefore the former is energetically more favorable than the latter.

To illustrate the charge transfer from Cs adsorbates to the substrate, we show the difference electron density of DC_C1 for Cs/GaAs(110) in Fig. 3 The difference electron density is defined as

$$\Delta\rho = \rho(2Cs/GaAs) - \rho(GaAs) - \rho(2Cs). \quad (2)$$

As shown in Fig. 3 there is a large charge-density accumulation along the dangling bond on b-Ga while little change occurs along the dangling bonds on the other surface Ga. There is also a charge depletion region around the two Cs adsorbates (Fig. 3). Clearly charge transfer occurs from the adsorbates to the dangling bond on b-Ga. The derelaxation around b-Ga is a manifestation of the saturation of its dangling bond. We also observe the charge redistribution around As and Ga in the topmost layer. Now several experimental observations can be qualitatively explained. Due to the saturation of the dangling bond on b-Ga and the surface derelaxation, Cs adsorption occurs at two "symmetrical" (both close to cation) but nonequivalent sites and two components in the Cs core levels are expected to be observed in UPS.[9,31] The extra components in anion and cation core levels result from the b-cation direct bonding to Cs, and the charge redistribution on surface anions and cations.[31] As the charge transfer from the AM adsorbates is localized on the dangling bonds on b cations, the AM chains exhibit an insulating behavior[8,25,26,29] even though the chains are composed of the most active metals.

The substrate derelaxation induced by Cs adsorption implies an effective interaction between the adjacent Cs atoms in a dimer mediated by the substrate. To further investigate this interaction, we perform calculations with two Cs atoms on a GaAs(110) 4×4 surface cell. The results show that the Cs atoms tend to get close to each other to form stable dimers within a reduced 2×2 region. Moreover, if the two Cs atoms are adsorbed in a 2×2 region, the geometries with one Ga outward are more stable, as described above; if it is not the case, the geometries with one Ga outward become unfavorable because charge transfer over a long distance is energetically costly. The behavior of the two Cs adsorbates
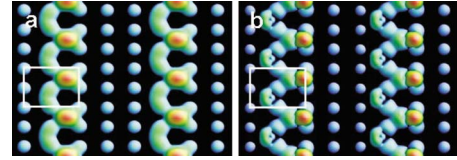
FIG. 4. (Color online) Simulated STM images at a bias voltage of −2 V for (a) Na and (b) Cs chains on GaAs(110) surface based on the building block proposed in the paper. The white rectangle indicates a 2×2 surface cell. The small spots between chains correspond to the topmost layer of As atoms. The enhancement of the signals of surface As underlying the chains due to the AM adsorption can be clearly seen.

on a 4×4 cell clearly suggests an effective short-range attractive interaction within a dimer mediated by the substrate outward b-Ga.

B. Formation of alkali-metal chains and interactions among the building blocks

To investigate the chain direction, we calculate the total energy of a Cs row on a GaAs(110) 4×4 supercell with two DC_C1s aligned along $[1-1\ 0]$ and interchain distance equal to $2a_0$ {a_0 is the lattice constant in the [001] direction}, corresponding to coverage $\theta_{Cs}=1/8$ ML. In comparing the total energy of $[1-1\ 0]$ structure to that of [001] structure in which two DC_C1s align along the [001] direction, we find the former is more favorable than the latter by an energy difference of 0.11 eV (0.06 eV per dimer complex). We also calculate various chain structures constituted by different dimer complexes oriented in either $[1-1\ 0]$ or [001] direction. Among all the considered structures, the $[1-1\ 0]$ chain composed of DC_C1 is the most favorable. The density functional theory (DFT) calculations are consistent with experiments and the assignment of DC_C1 as the building block of AM chains is further confirmed.

Figure 4 shows the simulated STM patterns for Na/GaAs(110) and Cs/GaAs(110) based on the $[1-1\ 0]$ chain structures described above. We can clearly see the difference between the Na and Cs chains. Besides the enhancement of the features of the topmost As atoms underlying the AM chains, there is only one spot in a 2×2 unit for Na chains [see Fig. 4(a)], corresponding to the Na atom close to the b-Ga, or more precisely, to the occupied dangling bond on b-Ga, while little feature is detectable for the other Na adsorbate. However, there are two inequilibrium bright spots in a 2×2 unit for the Cs chains [Fig. 4(b)] related to two Cs adsorbates in a unit. These patterns are in good agreement with the Na linear chains[25] and the Cs zigzag chains[7,26] observed by STM. The difference between Na and Cs chains may be attributed to the different charge redistribution within the system that depends on the details of the AM-surface interactions.

Charge transfer from the AM adsorbates to the substrate cations induces a surface dipole in each building block and the long-range electrostatic interactions among the building blocks may have an impact on the self-assembly of the AM chains. To understand the underlying relationship, we calcu-
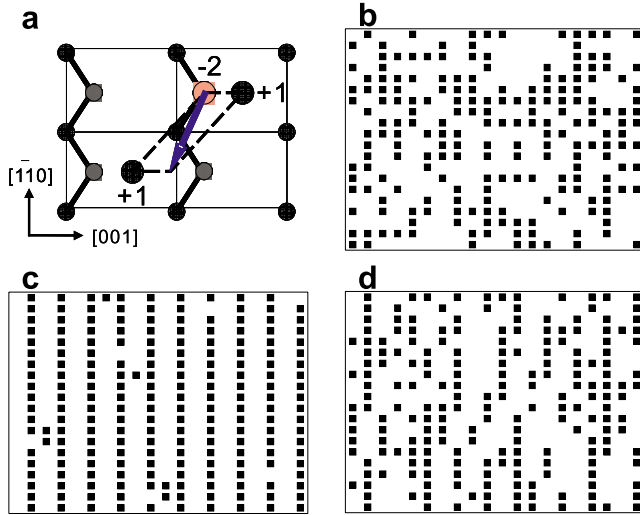
FIG. 5. (Color online) (a) Surface dipole (denoted by a blue arrow) induced by charge transfer from Cs adsorbates to substrate *b*-Ga atom. The numbers denote the nominal point charges assigned to the *b*-Ga and Cs atoms. The legends for atoms are the same as in Fig. 2. (b) The initial random distribution of building blocks on a 20×20 lattice, and the final equilibrium distribution at (c) 150 and (d) 300 K in the Metropolis Monte Carlo simulations for Cs chain formation at $\theta_{Cs} = 1/8$ ML. Each point represents a building block, i.e., a 2×2 surface cell.

late the surface dipole and the interaction energy among the building blocks from a simple model of point charges[34] for the Cs/GaAs(110) system. We assign a nominal charge of -2 to the *b*-Ga and a charge of $+1$ to each of the two Cs atoms [see Fig. 5(a)]. The surface dipole has a larger component in the $[1-1\ 0]$ direction. According to the dipole-dipole interaction, one may expect that the dipoles will attract each other when aligning along $[1-1\ 0]$ and repulse each other when along $[001]$, and this qualitatively explains why the building blocks tend to organize in the $[1-1\ 0]$ direction.

The electrostatic interactions between two building blocks can be represented by the Madelung energy of point charges,

$$E = \frac{1}{2\varepsilon} \sum_{i,j}{}' \frac{Q_i Q_j}{|R_i - R_j|}, \tag{3}$$

where Q_i is the charge of the *i*th atom at position R_i and ε is the effective dielectric constant, which we take to be the value of bulk GaAs, i.e., $\varepsilon = 13$. We focus on the Coulomb interactions between building blocks and do not consider the interaction within the building block itself. For simplicity, the structure variation of the building blocks in different environments is ignored. First, we calculate the interaction energy between different building blocks within a single chain. For a chain aligning in $[1-1\ 0]$, the interaction energy per dimer complex is -0.032 eV, compared to 0.050 eV for the $[001]$ chain. Here the minus sign indicates an effective attraction between DC_C1s along $[1-1\ 0]$ while the positive sign suggests a repulsion along $[001]$. Therefore the building blocks prefer to align along the $[1-1\ 0]$ direction rather than $[001]$. Second, we study the electrostatic energy between different $[1-1\ 0]$ chains that are supposed to be uni-

formly distributed in $[001]$ direction. When the chains are neighboring to each other, the energy per dimer complex is 0.111 eV. When the interchain distance increases to $2a_0$, $3a_0$, and $4a_0$, the value decreases to 0.067, 0.058, and 0.055 eV, respectively. This clearly indicates a long-range repulsive interaction between chains, decaying slowly with respect to the interchain distance.

The above DFT calculations and the Madelung energy can only provide the static information. We have also performed Metropolis Monte Carlo simulations to study the thermodynamic properties of the AM chains. The results with $\theta = 1/8$ ML on a 20×20 lattice are shown in Figs. 5(b)–5(d) with each point representing a building block. The interaction between building blocks is approximated by dipole-dipole interaction. Starting from a random distribution as shown in Fig. 5(b), the equilibrium configurations are obtained at different temperatures. At a low temperature $T = 150$ K, the building blocks form well-ordered $[1-1\ 0]$ long chains [Fig. 5(c)]. As the temperature increases, thermodynamics starts to disturb the chains. At room temperature ($T = 300$ K), most chains break into smaller pieces as shown in Fig. 5(d). At even higher temperatures, there are few well-defined $[1-1\ 0]$ chains. Simulations with a larger 40×40 lattice exhibit similar behaviors. From the Monte Carlo simulations we conclude that the electrostatic interactions among the building blocks serve as a driving force of the self-assembly of the AM chains at low and room temperatures.

C. Na adsorption on GaAs(110) at different coverage

In order to investigate the coverage dependence of adsorption, we have calculated the configurations of Na on a GaAs(110) 2×2 supercell at different coverage with the number of adsorbates N ranging from one to twelve, corresponding to coverage from $\theta_{Na} = 1/8$ to 3/2 ML. At intermediate and high coverages ($N > 3$), the structures of the adlayer become too complex to be interpreted by only one type of building block as the AM chains. However, the adlayer still exhibits some common characteristics. The Na adsorbates always preferentially occupy the S1 sites and then the S2 sites. More intriguingly, by adding every two Na adsorbates, there will be one more underlying Ga moving outward, as required by the GEC rule, because every two electrons can saturate one dangling bond on Ga. This fact further confirms that the surface derelaxation is a consequence of the saturation of dangling bonds on Ga induced by AM adsorption. All the four dangling bonds on Ga will be filled at $N = 8$. The saturation of the first layer also occurs at $N = 8(\theta_s = 1$ ML) and the oncoming Na atoms will set off the growth of a second layer. We point out here that it is only a coincidence that the saturation of all the dangling bonds on Ga happens to occur at θ_s for Na/GaAs(110). It is not always the case for every AM/III–V (110) system, as we will see below for Cs/GaAs(110).

The formation energy per Na adsorbate as a function of coverage has been calculated and is plotted in Fig. 6. The formation energy is defined as

$$E_{form} = (E_{tot} - E_{sub} - N \times \mu_{Na})/N, \tag{4}$$

where E_{tot} is the total energy of the slab including the adsorbates, E_{sub} the energy of the substrate only, and μ_{Na} the
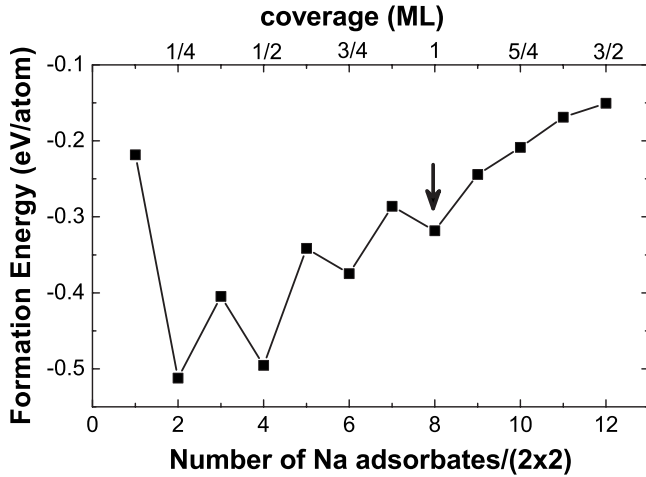
FIG. 6. Formation energies per adsorbate for Na on a GaAs(110) 2×2 surface cell as a function of coverage. The arrow indicates the saturation coverage and is also the transition points from 2D to 3D growth. The lines are only a guide to the eye.

chemical potential of Na metal. The formation energy shows an even-odd oscillation superimposed on a rising curve up to θ_s, reaching a local minimum at every even number, a local maximum at every odd number, and a global minimum at $N=2$. This oscillatory behavior indicates that Na atoms tend to form stable pairs and the pair will repel the oncoming single adsorbate or other pairs nearby. For 3D growth ($N > 8$), E_{form} goes up monotonically as N increases. The oscillation of E_{form} can be well explained by the GEC rule. When there are odd-number Na adsorbates that can only donate odd-number electrons, some dangling bonds on Ga must be half filled, corresponding to a relatively unfavorable structure. When there are even-number adsorbates providing even-number electrons, the dangling bonds on Ga will either be fully filled or remain empty, leading to a more stable configuration.

A similar calculation has been carried out for Cs/GaAs(110). In contrast to Na, the first Cs adlayer saturates at $N=4$, i.e., $\theta_s = 0.5$ ML, which is close to the experimental value of 0.55 ML.[30] The difference in θ_s between Na and Cs is due to their different sizes. In the 2D growth region ($N < 4$), one more underlying Ga moves outward by increasing every two Cs adsorbates, same as the Na case. For 3D growth ($N > 4$), no more surface Ga atoms move outward by increasing Cs coverage. Therefore the second Cs layer interacts mainly with the first Cs layer and do not transfer the valence electrons to surface Ga. Based on these findings, a simple picture can be drawn to describe the interactions between AM adsorbates and substrate. In 1D chain and 2D adlayer, AM atoms transfer their s electrons to the substrate and become partially ionized. Due to the localization of the transferred electrons at the rehybridized orbitals of Ga, 1D AM chain and 2D adlayer present nonmetallic feature. We consider the case that the bonding between the AM adsorbates and the substrate is largely ionic. However, upon the growth of a second AM layer, which is metallically bonded to the first layer, the 3D adlayer shows metallic feature and the GEC rule is not applicable to these systems.

V. TRIVALENT AND PENTAVALENT METALS ADSORPTION ON GaAs

The III–V heterostructures are widely studied for surface segregation and ordering, which are key to achieve abrupt interfaces in these systems. The group-III metals such as In and Al are isovalent, and close in electronegativity to Ga (see Fig. 1). These metals are supposed to occupy the Ga lattice sites and act just like Ga, as far as the electron counting is concerned. Thus the GEC rule in these systems is a simple extension of the classic EC rule. A number of experiments on InGaAs and AlGaAs (Refs. 35 and 36) showed that In (Al) atoms occupy the Ga sites. Due to the size effects, the local strain distorts the In (Al)-As bonds and results in the In-In (Al-Al) anisotropic pair correlations.[37] A first-principles calculation on a similar system GaInP (Ref. 38) studied a set of GaAs(001) stable reconstructions satisfying the EC rule but with P replacing As, and various patterns of Ga and In occupying the Ga surface sites.

Similarly, Sb and Bi are isovalent, and are close in electronegativity to As (see Fig. 1). These metals are expected to behave as As, leading to another natural extension of the classic EC to the GEC rule. In experiments complex reconstruction patterns were observed on Sb covered GaAs surfaces with Sb at substitutional sites. The Sb-terminated GaAs(001)-$\beta 2(2 \times 4)$ surface after annealing can return to a (2×4) reconstruction with Sb dimers substituting As dimers,[39] satisfying the GEC rule. On the Sb-terminated GaAs(111)B-(2×2) surface, there are more complex Sb chain pairs between which Sb trimers substitute As trimers in various patterns. Several models obeying the GEC rule have been proposed to describe these complex structures, among which the (3×8) reconstruction is in good agreement with the STM images.[40] On the other hand, the reconstruction of Bi-terminated GaAs(111)B surface is much more straightforward. In the $c(4 \times 2)$ pattern, Bi trimers replace As trimers at T_4 sites with the As rest atoms unaffected, fulfilling the GEC rule.[41]

VI. Mn ADSORPTION ON GaAs(001)

DMS is an important class of materials for the development of semiconductor-based spintronics. To grow optimal epitaxial GaAsMn films and to increase the Curie temperature, it is important to understand the Mn induced reconstructions at the initial growth stages. It is thought that transition metals will bring more complexities to the surface reconstructions due to their active diffusive d electrons. We next apply the GEC rule to Mn/GaAs(001), extending its application to transition metals.

According to the GEC rule, Mn adsorbates should preferentially occupy the interstitial sites and act as donors on the GaAs(001) surface. At the low Mn coverages considered in the present work, the valence electrons in a Mn adsorbate atom resemble those of an isolated Mn atom, given by $3d^5 4s^2$. The Mn atom would try to donate its two s electrons while leaving its half-filled d-band intact, which has been confirmed by our first-principles calculations. Thus in the case of Mn, n_R is just the number of electrons in the d states and is correlated with the local magnetic moment of Mn

atoms. A simple formula can be drawn to calculate local magnetic moment from n_R:

$$\mu_{LMM} = \sum_i |\mu_{Mn,i}| = n_R - 2n_{d\downarrow}, \tag{5}$$

where μ_{LMM} is the total local magnetic moment of a surface unit cell, $\mu_{Mn,i}$ the local magnetic moment of the ith Mn atom in the unit cell, and $n_{d\downarrow}$ the number of electrons in the minority spin-down states. Similar to the classic EC model, here the net charge transfer from the metal adsorbates to the substrate is nominal. That is, upon metal adsorption, the metal valence electrons mainly occupy the substrate-induced states, which are spatially localized on the surface atoms. Therefore, the metal/semiconductor system remains largely charge neutral near the surfaces.

As is well known, on As-terminated GaAs(001) surface, there is a lack of one electron for each As dimer, which may accept electrons from Mn adsorbates. STM images of Mn covered GaAs(001) surface present a 2×2 symmetry.[12] Thus in this paper we focus on the reconstructions of GaAs(001) 2×2 surface induced by Mn adsorption. We adopt the same way to name the reconstruction based on two simple motifs, as in Ref. 12: the bridge site interstitial for Mn is named as β motif, the hollow site interstitial is named as γ motif, and the subscript (lmn) indicates surface Mn/Ga/As coverage with respect to the ideal As-terminated GaAs(001) 2×2 surface.

A. $\theta_{Mn} = 1/4$ ML

The simplest structures for 1/4 ML coverage of Mn are those with one Mn atom on an ideal 2×2 surface. One of such structures, β_{100}, where the Mn atom is located below one of the As dimers, is shown in Fig. 7. The As-As bond above the Mn atom is slightly strained but remains unbroken. The application of the GEC rule to this reconstruction is straightforward. There is a lack of two electrons on the ideal As-terminated 2×2 surface and the two s electrons donated by the Mn atom can stabilize the surface, leading to the optimal $n_R = 5$ for Mn. The local magnetic moment obtained from DFT calculation is also $5\mu_B$.

The low-energy reconstructions at 1/4 ML coverage are the γ structures. Figure 7 shows the structure of γ_{102} where one more As dimer is positioned on the ideal 2×2 surface and the Mn atom has four neighboring As atoms in plane. Within the counting slab, as shown in Fig. 7, we have $n_{Mn} = 1$, $n_{As} = 4/2 + 2 = 4$, and $n_{Ga} = 0$. Note that the atoms on the edge of the counting slab have to be counted as half since they only contribute half of their electrons to the slab. There are five σ bonds and six occupied dangling bonds on As atoms. By applying Eq. (1), we obtain $n_R = 7 \times 1 + 5 \times 4 - 2 \times 11 = 5$, which is the optimal value of n_R required by the GEC rule. One can obtain the γ_{111} phase, a variant of γ_{102}, by replacing one topmost As atom with Ga atom. Accordingly the total number of electrons in γ_{111} is less than that of γ_{102} by two. Meanwhile, the dangling bond on Ga is empty so the required number of electrons is less by two as well. Hence the GEC rule holds for the γ_{111} structure. A similar argument can be applied to another variant, i.e., the γ_{102} structure, where the topmost As dimer is replaced by a Ga
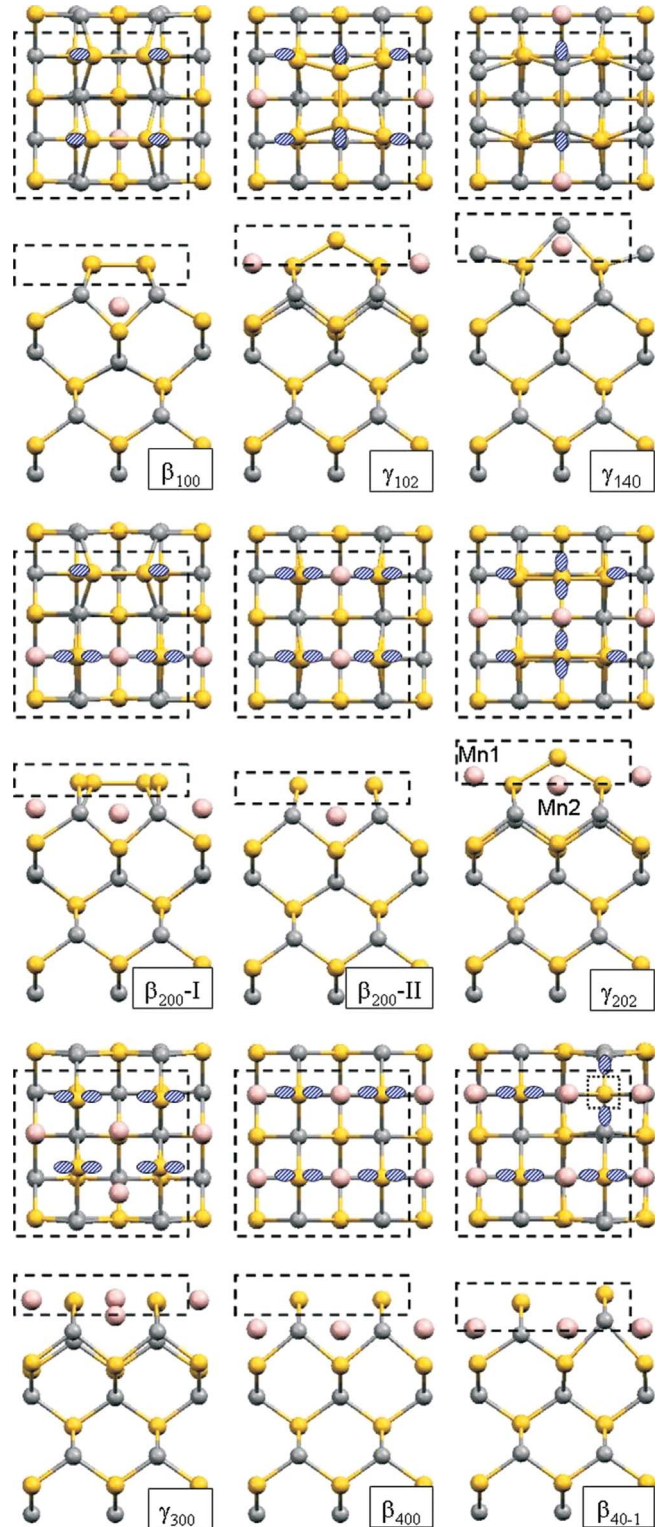
FIG. 7. (Color online) Top and side views of the calculated low-energy 2×2 reconstructions of the GaAs(001) surface induced by Mn adsorbates at various coverage. The yellow, gray, and pink balls are As, Ga, and Mn atoms, respectively. All the occupied dangling bonds on surface As and Ga are denoted by hatched ellipses. The counting slab is depicted as a dashed square. The As vacancy in β_{40-1} is denoted by a dotted square.

dimer. The local magnetic moments for these structures from DFT are all $5\mu_B$. The calculations revealed that for θ_{Mn} =1/4 ML, the three γ phases are the most stable structures under As-rich, moderate As concentration, and As-poor conditions, respectively.[12]

Another interesting structure is γ_{140} where one Mn atom adsorbs on an ideal Ga-terminated 2×2 substrate. It can be seen from Fig. 7 that the Ga dimer next to the Mn atom moves higher than the other Ga dimer by about 0.5 Å, indicating that the dangling bonds on the former are filled, as in the case of AM/GaAs. According to the classic EC rule, there are two excessive electrons on the ideal Ga-terminated 2 $\times$2 surface. The Mn atom can donate two more electrons and the four electrons in total can just saturate two dangling bonds on Ga. Therefore on this surface we have n_R=5, again in good agreement with the DFT calculation. This structure is a good example of charge transfer from Mn donor to the surface Ga due to the difference in their electronegativities. The γ_{240} structure with two Mn atoms adsorbed on the ideal Ga-terminated 2×2 surface shows similar behaviors. Due to the addition of one Mn adsorbate, there are six more electrons that can fill three dangling bonds on Ga. Thus three topmost Ga atoms move higher than the other Ga atom in γ_{240}.[42]

B. $\theta_{Mn}=1/2$ ML

Figure 7 shows two configurations of β_{200} phase with different Mn adsorption sites. In β_{200}-I structure, one Mn atom is located below an As dimer and the other Mn atom is located in the trough between As dimer rows. The As dimer above the Mn atom is broken due to the strain. In β_{200}-II structure, the two Mn atoms are positioned below As dimers and break the two As dimers. By applying the GEC rule, for β_{200}-I we have $n_{Mn}=2$, $n_{As}=4/2=2$, and $n_{Ga}=0$. There are only one σ bond associated with the intact As dimer and six occupied dangling bonds on As atoms. By Eq. (1) one can obtain $n_R=7\times2+5\times2-2\times(1+6)=10$, or five electrons per Mn atom, and our calculation yields a local magnetic moment of $10\mu_B$ on this surface. As to the β_{200}-II structure, there is one less σ bond but two more occupied dangling bonds due to the two broken As dimers. Here Eq. (1) reads $n_R=8$, in agreement with the calculated local magnetic moment of $8\mu_B$. In other words, the β_{200}-I reconstruction satisfies the GEC requirement, i.e., $n_R=5$ per Mn atom, while β_{200}-II does not. Our calculations showed that β_{200}-I is energetically more stable than β_{200}-II by 0.8 eV. In general, the reconstructions satisfying the GEC rule are more stable than those against it.

A low-energy structure at 1/2 ML coverage under As-rich conditions is the γ_{202} phase with two more As atoms and two Mn adsorbates (denoted by Mn1 and Mn2 in Fig. 7) on an ideal As-terminated 2×2 surface. The two added As atoms do not bond to each other due to the strain induced by the Mn2 atom below them. On this surface we have $n_{Mn}=2$, $n_{As}=4/2+2=4$, $n_{Ga}=0$, $n_{bonds}=n_{\sigma\text{-bonds}}+n_{ODBs}=4+8=12$, and thus $n_R=7\times2+5\times4-2\times12=10$, reaching the optimal valence state of Mn. However the calculated local magnetic moment of this structure is $8\mu_B$. According to Eq. (5) this
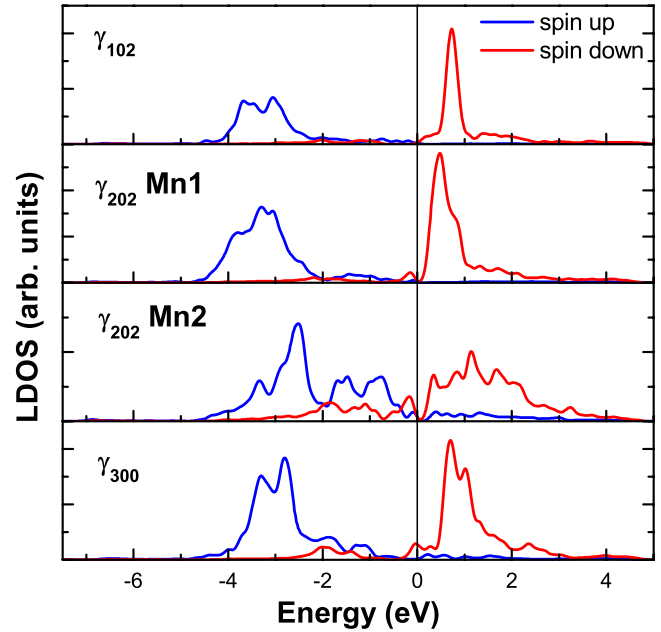
FIG. 8. (Color online) LDOS of Mn d bands near the Fermi level (set to zero) in γ_{102}, γ_{202}, and γ_{300}. The s and p components are too weak and not shown here. The overlap between the spin-up and spin-down states in the two lower panels is a consequence of the strong Mn-As and Mn-Mn interactions, respectively.

implies $n_{d\downarrow}\neq0$. In Fig. 8 we show the local density of states (LDOS) on Mn atoms in this structure, comparing to those of the γ_{102} structure. The s and p components are extremely weak and ignored in the figures. It can be easily seen that the Mn spin-up and spin-down states in γ_{102} are well separated, and no spin-down states are occupied, corresponding to $n_{d\downarrow}$ =0. For γ_{202}, the LDOS of Mn1 atom presents similar features except for the shift of the peaks. However, the LDOS of Mn2 is quite different. Besides the great change in the shape, the spin-up and spin-down states are overlapped with each other, and the spin-down states become partially occupied. We notice that the local environment of Mn1 is quite similar to that in γ_{102} with four neighboring As atoms in plane while the Mn2 atom has six neighboring As atoms. Therefore the overlap of spin-up and spin-down states of Mn2 atom is induced by the strong Mn-As interactions.

The simulated STM image for γ_{202} shown in Fig. 9(a) agrees well with the experiment.[12] We should emphasize that the two bright dots in a unit cell correspond to the topmost As atoms rather than the Mn atoms themselves. In fact, the
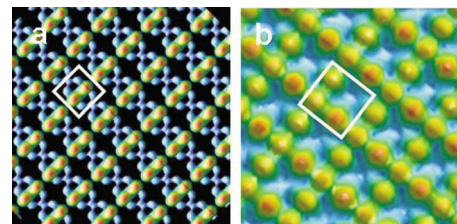
FIG. 9. (Color online) The simulated STM images for (c) γ_{202} and (d) β_{40-1} structures. The white rectangle indicates a 2×2 surface cell.

simulated STM image of γ_{102} (not shown) presents similar patterns except for the different distance between the surface As atoms. More information such as the coverage of Mn is needed to determine the exact structure observed by experiments.

C. $\theta_{Mn}=3/4$ ML

The γ_{300} structure has the lowest energy at this coverage. Due to the strain effects, the σ bonds of the two As dimers are all broken, as is shown in Fig. 7. The number of occupied dangling bonds on As atoms increases to eight, reaching the maximal value. In addition, one of the Mn atoms deviates from the hollow site, having two Ga and two As nearest neighbors instead of four As nearest neighbors. The LDOS of the d bands on this Mn atom is shown in Fig. 8. The LDOS on the other two Mn atoms exhibits similar features. Applying the GEC rule to this surface, we have $n_{Mn}=3$, $n_{As}=4/2$ $=2$, $n_{Ga}=0$, $n_{bonds}=n_{ODBs}=8$, and $n_R=7\times3+5\times2-2\times8$ $=15$, i.e., five electrons per Mn atom. However, the calculations derive a local magnetic moment of $13\mu_B$ on this surface, indicating that $n_{d\downarrow}=1$ according to Eq. (5). This is indeed the truth as seen from Fig. 8, where the overlap between the spin-up and spin-down states results in partial occupation of the spin-down states. In general, our DFT calculations for more than ten model structures at 3/4 ML coverage always yield $n_{d\downarrow}=1$.[42] Therefore at high coverage ($\theta_{Mn}>1/2$ ML), the Mn-Mn interactions become important, and cause the overlap between the spin-up and spin-down states. It is anticipated that the overlap will be greater at higher coverage, corresponding to larger values of $n_{d\downarrow}$, which will be testified below at $\theta_{Mn}=1$ ML.

D. $\theta_{Mn}=1$ ML

Figure 7 shows the β_{400} structure where the bonds of As dimers are all broken due to the strain effect, as in the case of γ_{300}. The number of As, Ga, and bonds in β_{400} is the same as that in γ_{300} except that $n_{Mn}=4$. Thus we have $n_R=7\times4+5$ $\times2-2\times8=22$, i.e., 5.5 electrons on each Mn atom. The calculation of local magnetic moment yields $18\mu_B$, corresponding to $n_{d\downarrow}=2$. Clearly, n_R is higher than the optimal value required by the GEC rule and we may search for more stable reconstructions by lowering the value of n_R.

One way to lower the value of n_R is to remove one topmost As atom from β_{400}, leaving an As vacancy on the surface. Figure 7 shows the β_{40-1} phase where the As vacancy is indicated by a dotted square. There are two exposed dangling bonds on the second layer of Ga atoms that should be filled according to the GEC rule. Here we have $n_{Mn}=4$, $n_{As}=3$, $n_{Ga}=4/2=2$, $n_{bonds}=n_{\sigma-bonds}+n_{ODBs}=6+8=14$, and thus n_R $=7\times4+5\times3+3\times2-2\times14=21$, i.e., 5.25 electrons per Mn atom. Although this is not the optimal n_R required by the GEC rule, it is the nearest one toward the optimal value in our studies. Our DFT calculations showed that the β_{400} and β_{40-1} are both low-energy structures at this coverage, and the latter is energetically more favorable than the former under As-poor conditions.[12] The DFT calculation derived a local magnetic moment of $17\mu_B$ on this surface, i.e., $n_{d\downarrow}=2$, the same as in β_{400}. The LDOS of Mn d band reveals an over-

lapping between the spin-up and spin-down states as well. In fact, we always obtain $n_{d\downarrow}=2$ for other structures at θ $=1$ ML. In Fig. 9(b) we show the simulated STM image based on β_{40-1}, which is in good agreement with the experimental observation.[12]

E. Summary of the Mn/GaAs(001) system

We can draw the following conclusions on the ground of above results for Mn induced GaAs(001) surface reconstructions under the guidance of the GEC rule: (i) The optimal value of n_R is five per Mn atom. The stable reconstructions will be those that take the optimal or the possible closest value to the optimal n_R. (ii) There is a relationship between n_R and local magnetic moment. However, strong Mn-As or Mn-Mn interactions will cause the overlapping of the spin-up and spin-down states of Mn d bands, leading to a nonzero $n_{d\downarrow}$. The exact value of $n_{d\downarrow}$ depends on the specific interactions that may involve the complex spin-spin interactions, which is beyond the GEC rule. (iii) Comparing the GEC rule to the DFT calculations, we have, when there are no strong Mn-As interactions, $n_{d\downarrow}=0$ at $\theta_{Mn}=1/4$ and 1/2 ML, $n_{d\downarrow}=1$ at 3/4 ML, and $n_{d\downarrow}=2$ at 1 ML. (iv) The Mn adsorbates only serve as donors on the surface and are not involved in bond formation with other atoms. But the strain effect induced by the adsorption of Mn may break the surface dimers, leading to the change of the number of σ bonds and occupied dangling bonds. (v) The dangling bonds on As atoms are always filled while those on Ga atoms may be filled if they are in close contact to Mn atoms. How many dangling bonds on Ga will be occupied depends on the number of the remaining electrons on the surface after filling all the σ bonds and the dangling bonds on As.

VII. Au ADSORPTION ON GaAs(001)

Gold is a metal widely used in the formation of metallic contacts on semiconductors. From a crude analysis of the GEC rule, Au is expected to behave as an acceptor on the GaAs(001) surface due to its higher electronegativity than both As and Ga. In fact, Au exhibiting a negatively charged state on surface is not an unusual phenomenon. A theoretical study on the catalysis of Au particles supported by MgO(110) showed a sizable charge transfer from the surface oxygen atoms to Au.[43] Experimentally it is possible to control the charge state of individual Au atoms on NaCl(100)/Cu(111) from neutral to negatively charged state with a STM tip.[44]

We have studied the Au adsorption on both GaAs(001) Ga-terminated and As-terminated surfaces. The Au adsorbate prefers to occupy the substitutional sites as expected. When Au is positioned on top of a Ga or As dimer, it always breaks the underlying dimer even at very low coverage. The distance between Au and the neighboring Ga or As atoms is about 2.5 Å. The LDOS analysis demonstrates a strong hybridization between Au and its neighboring surface atoms. Moreover, the difference electron densities show electron accumulation between Au and its neighboring Ga or As while electron depletion occurs near the involved atoms. All these
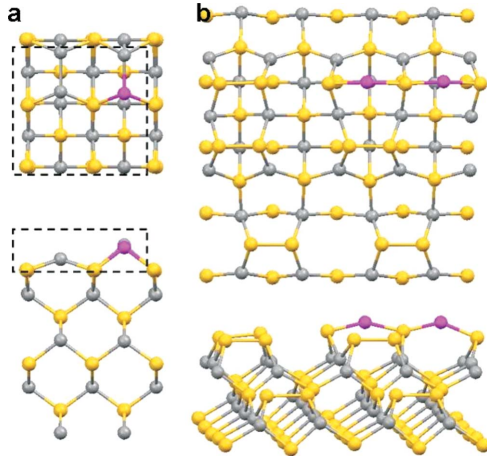
FIG. 10. (Color online) (a) Top and side views of the structure with one Au atom replace one surface Ga atom on an ideal Ga-terminated 2×2 cell. (b) The lowest-energy structure with two Au atoms on As-terminated 4×4 surface. The yellow, gray, and magenta balls represent As, Ga, and Au atoms, respectively.

observations indicate that the Au adsorbate forms covalent bonds with the surface atoms. Due to the formation of the covalent bonds, there is some difference in electron counting from the systems studied in previous sections. Take Cs/GaAs(110) as an example for comparison. The Cs adsorbates act as electron donors and the donated electrons occupy the Ga-derived dangling bonds. In other words, the Ga-derived dangling-bond states are shifted below the Fermi level upon Cs adsorption while the Cs s states are above the Fermi level, which has been confirmed by LDOS analysis. When applying the GEC rule, we include the Ga dangling bonds. Here in Au/GaAs system, the Au-Ga or Au-As bonding states are present below the Fermi level. Therefore, when counting the number of bonds, we should also include the Au-Ga or Au-As bonds.

Figure 10(a) shows the structure with one Au atom replacing one surface Ga atom on an ideal Ga-terminated 2×2 cell. In the counting slab, we have $n_{Au}=1$, $n_{As}=4/2=2$, $n_{Ga}=3$, and $n_{bonds}=n_{\sigma\text{-bonds}}+n_{OBDs}=(7+3)+0=10$. Here the surface Ga and As atoms form seven σ bonds while the Au adsorbate is involved in three bonds. From Eq. (1) we obtain $n_R=(1 \times 1+5 \times 2+3 \times 3)-2 \times 10=0$, i.e., the surface electrons just occupy all the surface bonds. Figure 10(b) displays the lowest-energy structure with two Au atoms on As-terminated 4×4 surface, that is, two GaAs(001)-$\beta 2(2 \times 4)$ unit cells. The Au atom located in the trough forms covalent bonds with two As atoms that originally have one occupied dangling bonds on each of them. The other Au atom breaks the underlying As dimer and also forms two Au-As bonds. Two electrons from Au and the other two from the broken As-As bond just provide the right number of electrons required by the GEC rule. Four Au atoms can adsorb near two adjacent As-As dimers in a similar way. Compared to a previously proposed structure where a Au$_4$ cluster adsorbs on top of two adjacent As-As dimers,[45] the structure suggested here is energetically more favorable by 3.6 eV and is consistent with the STM observation.[46]

Each Au atom has only one s electron but can form two or three σ bonds with the GaAs surface. There must be some charge transferred from the surface to the Au adsorbates. Therefore Au acts as an electron acceptor on GaAs substrate. Here $n_R=0$ means that there are no spare electrons on Au because all the electrons are involved in covalent bonding. However, it is not straightforward to deduce how many electrons are transferred from the substrate to Au due to the covalent bonding nature. Finally we want to emphasize that the strain effects may also play an important role in determination of Au induced surface reconstructions especially at high coverage, which is thought to be beyond the GEC rule.

VIII. CONCLUSIONS

We have discussed in detail a generalized electron counting rule as a generic guiding principle to the metal-induced compound semiconductor surface reconstructions. In this picture, the metal adsorbates serve as an electron bath, either denoting or accepting the right number of electrons for the binary host system to choose a specific reconstruction form within the framework of the classic EC model. In the meanwhile, the metal adsorbates select an optimal valence state. Specially, if metal forms covalent bonds with the substrate, these bonds must be included when counting the electrons. The validity of the GEC rule have been justified by its application to various reconstructions induced by a wide range of metal adsorbates on different GaAs surfaces, based on comprehensive first-principles calculations and available experiments. AMs act as electron donors on the GaAs surface. Under the guidance of the GEC rule, the building block of the AM chains is identified and the surface derelaxation and self-assembly mechanisms are well explained. The behavior of the adlayers up to the saturate coverage also obeys the GEC rule. Group-III and group-V metals on GaAs surface behave just like Ga and As, respectively, and in this case the GEC rule is just a simple extension of the classic EC model. For magnetic adsorbates Mn, the GEC rule can predict possible low-energy reconstructions over a wide range of coverage which can be confirmed by DFT calculations and further experiments. Moreover, the GEC rule provides an intrinsic link between the reconstruction structure and the local magnetic moments of Mn adsorbates. The electron counting technique can also be applied to other metal adsorbates such as Au that forms strong covalent bonds with the substrate. Although GaAs is used as a prototype of the substrate in our present study, the GEC rule as a generic principle is expected to be applicable to other compound semiconductors.

¹ D. J. Chadi, J. Vac. Sci. Technol. A **5**, 834 (1987); M. D. Pashley, Phys. Rev. B **40**, 10481 (1989).

² Charles B. Duke, Chem. Rev. (Washington, D.C.) **96**, 1237 (1996).

³ Q. K. Xue, T. Hashizume, and T. Sakurai, Prog. Surf. Sci. **56**, 1 (1997); S. H. Lee, W. Moritz, and M. Scheffler, Phys. Rev. Lett. **85**, 3890 (2000); W. G. Schmidt, P. H. Hahn, F. Bechstedt, N. Esser, P. Vogt, A. Wange, and W. Richter, *ibid.* **90**, 126101 (2003).

⁴ K. W. Haberern and M. D. Pashley, Phys. Rev. B **41**, 3226 (1990); M. D. Pashley and K. W. Haberern, Phys. Rev. Lett. **67**, 2697 (1991); D. Martrou, J. Eymery, and N. Magnea, *ibid.* **83**, 2366 (1999).

⁵ H. H. Farrell, J. P. Harbison, and L. D. Peterson, J. Vac. Sci. Technol. B **5**, 1482 (1987).

⁶ H. Ohno, Science **281**, 951 (1998); T. Dietl, H. Ohno, F. Matsukura, J. Cibert, and D. Ferrand, *ibid.* **287**, 1019 (2000); S. A. Wolf, D. D. Awschalom, R. A. Buhrman, J. M. Daughton, S. von Molnár, M. L. Roukes, A. Y. Chtchelkanova, and D. M. Treger, *ibid.* **294**, 1488 (2001).

⁷ P. N. First, R. A. Dragoset, Joseph A. Stroscio, R. J. Celotta, and R. M. Feenstra, J. Vac. Sci. Technol. A **7**, 2868 (1989).

⁸ L. J. Whitman, J. A. Stroscio, R. A. Dragoset, and R. J. Celotta, Phys. Rev. B **44**, 5951 (1991).

⁹ S. Modesti, A. Falasca, M. Polentarutti, M. G. Betti, V. De Renzi, and C. Mariani, Surf. Sci. **447**, 133 (2000).

¹⁰ L. Gavioli, M. G. Betti, V. Corradini, and M. Sancrotti, Phys. Rev. B **70**, 125317 (2004).

¹¹ L. J. Whitman, B. R. Bennett, E. M. Kneedler, B. T. Jonker, and B. V. Shanabrook, Surf. Sci. **436**, L707 (1999).

¹² S. B. Zhang, L. X. Zhang, L. F. Xu, E. G. Wang, X. Liu, J. F. Jia, and Q. K. Xue, Phys. Rev. B **69**, 121308(R) (2004).

¹³ D. R. Heslinga, H. H. Weitering, D. P. van der Werf, T. M. Klapwijk, and T. Hibma, Phys. Rev. Lett. **64**, 1589 (1990); K. M. Schirm, P. Soukiassian, P. S. Mangat, and L. Soonckindt, Phys. Rev. B **49**, 5490 (1994); V. Yu. Aristov, G. Le Lay, M. Grehk, V. M. Zhilin, A. Taleb-Ibrahimi, G. Indlekofer, and P. Soukiassian, Surf. Rev. Lett. **2**, 723 (1995).

¹⁴ G. Allan and M. Lannoo, Phys. Rev. Lett. **66**, 1209 (1991).

¹⁵ L. X. Zhang, E. G. Wang, Q. K. Xue, S. B. Zhang, and Z. Y. Zhang, Phys. Rev. Lett. **97**, 126103 (2006).

¹⁶ G. Kresse and J. Hafner, Phys. Rev. B **47**, 558 (1993); **49**, 14251 (1994).

¹⁷ J. P. Perdew and Y. Wang, Phys. Rev. B **33**, 8800 (1986).

¹⁸ P. E. Blöchl, Phys. Rev. B **50**, 17953 (1994); G. Kresse and D. Joubert, *ibid.* **59**, 1758 (1999).

¹⁹ H. J. Monkhorst and J. D. Pack, Phys. Rev. B **13**, 5188 (1976).

²⁰ D. Vanderbilt, Phys. Rev. B **41**, 7892 (1990).

²¹ R. J. Wilson and S. Chiang, Phys. Rev. Lett. **58**, 369 (1987); I. K. Robinson, P. A. Bennett, and F. J. Himpsel, *ibid.* **88**, 096104 (2002); D. Sánchez-Portal and R. M. Martin, Surf. Sci. **532-535**, 655 (2003).

²² S. C. Erwin and A. G. Petukhov, Phys. Rev. Lett. **89**, 227201 (2002); H. Wu, M. Hortamani, P. Kratzer, and M. Scheffler, *ibid.* **92**, 237202 (2004); W. G. Zhu, H. H. Weitering, E. G. Wang, E. Kaxiras, and Z. Y. Zhang, *ibid.* **93**, 126102 (2004).

²³ L. Pauling, *The Nature of the Chemical Bond and the Structure of Molecules and Crystals* (Cornell University Press, Ithaca, NY, 1939).

²⁴ M. G. Betti, V. Corradini, M. Sauvage-Simkin, and R. Pinchaux, Phys. Rev. B **66**, 085335 (2002).

²⁵ C. Bai, T. Hashizume, D. R. Jeon, and T. Salurai, Jpn. J. Appl. Phys., Part 2 **31**, L1117 (1992).

²⁶ L. J. Whitman, Joseph A. Stroscio, R. A. Dragoset, and R. J. Celotta, Phys. Rev. Lett. **66**, 1338 (1991).

²⁷ U. del Pennino, B. Salvarani, R. Compañò, and O. Pankratov, Phys. Rev. B **52**, 10717 (1995).

²⁸ J. Hebenstreit, M. Heinemann, and M. Scheffler, Phys. Rev. Lett. **67**, 1031 (1991); O. Pankratov and M. Scheffler, *ibid.* **70**, 351 (1993); O. Pankratov and M. Scheffler, *ibid.* **71**, 2797 (1993).

²⁹ N. J. DiNardo, T. M. Wong, and E. W. Plummer, Phys. Rev. Lett. **65**, 2177 (1990).

³⁰ T. Kendelewicz, P. Soukiassian, M. H. Bakshi, Z. Hurych, I. Lindau, and W. E. Spicer, J. Vac. Sci. Technol. A **6**, 1569 (1988).

³¹ G. Faraci, A. R. Pennisi, F. Gozzo, S. La Rosa, and G. Margaritondo, Phys. Rev. B **53**, 3987 (1996); M. G. Betti, V. Corradini, G. Gertoni, S. Gardonio, C. Mariani, L. Gavioli, R. Belkhou, and A. Taleb-Ibrahimi, Surf. Sci. **477**, 35 (2001).

³² A. Calzolari, C. A. Pignedoli, R. Di Felice, C. M. Bertoni, and A. Catellani, Surf. Sci. **454-456**, 207 (2000); A. Calzolari, C. A. Pignedoli, C. M. Bertoni, and A. Catellani, *ibid.* **491**, 265 (2001).

³³ H. Yi, H. Kim, B. Kuruvilla, and J. Chung, Phys. Rev. B **67**, 195302 (2003).

³⁴ J. E. Northrup and S. Froyen, Phys. Rev. B **50**, 2015 (1994); S. B. Zhang and Alex Zunger, *ibid.* **53**, 1343 (1996).

³⁵ J. F. Zheng, J. D. Walker, M. B. Salmeron, and E. R. Weber, Phys. Rev. Lett. **72**, 2414 (1994); M. Pfister, M. B. Johnson, S. F. Alvarado, H. W. M. Salemink, U. Marti, D. Martin, F. Morier-Genoud, and F. K. Reinhart, Appl. Phys. Lett. **67**, 1459 (1995); K.-J. Chao, C.-K. Shih, D. W. Gotthold, and B. G. Streetman, Phys. Rev. Lett. **79**, 4822 (1997).

³⁶ A. R. Smith, K.-J. Chao, C.-K. Shih, K. A. Anselm, A. Srinivasan, and B. G. Streetman, Appl. Phys. Lett. **69**, 1214 (1996).

³⁷ J.-H. Cho, S. B. Zhang, and A. Zunger, Phys. Rev. Lett. **84**, 3654 (2000).

³⁸ S. Froyen and A. Zunger, Phys. Rev. B **53**, 4570 (1996).

³⁹ P. Moriarty, P. H. Beton, Y.-R. Ma, M. Henini, and D. A. Woolf, Phys. Rev. B **53**, R16148 (1996); L. J. Whitman, B. R. Bennett, E. M. Kneelder, B. T. Jonker, and B. V. Shanabrook, Surf. Sci. **436**, L707 (1999).

⁴⁰ P. Moriarty, P. H. Beton, and D. A. Woolf, Phys. Rev. B **51**, 7950 (1995).

⁴¹ C. McGinley, A. A. Cafolla, B. Murphy, D. Teehan, and P. Moriarty, Appl. Surf. Sci. **152**, 169 (1999).

⁴² L. X. Zhang and E. G. Wang, Acta Phys. Sin. **55**, 142 (2006).

⁴³ L. M. Molina and B. Hammer, Phys. Rev. B **69**, 155424 (2004).

⁴⁴ J. Repp, G. Meyer, F. E. Olsson, and M. Persson, Science **305**, 493 (2004).

⁴⁵ A. Amore Bonapasta, G. Scavia, and F. Buda, Surf. Sci. **520**, 53 (2002).

⁴⁶ Z. Tang, S. Yang, W. Wang, J. F. Jia, E. G. Wang, and K. Wu, Chem. Phys. Lett. (to be published).